Fast-to-slow axis mode imaging for brightness enhancement of a broad-area laser diode array

Andrew M. Jones[*] and Juliet T. Gopinath

University of Colorado - Boulder, Department of Electrical, Computer and Energy Engineering, Boulder, CO, 80309, USA

[*]*andrew.mi.jones@colorado.edu*

Abstract: Broad-area laser (BAL) diodes have found use in numerous applications requiring multi-watt powers, but remain limited by poor spatial beam quality. A novel laser cavity that enhances the brightness of a BAL array has been demonstrated. Wavelength beam combining (WBC) is used to spatially overlap output from the emitters. Improved beam quality is achieved by imaging the fast-axis mode onto the slow axis of the BAL array. The brightness is enhanced twofold over a typical Littman-Metcalf WBC cavity, reaching 47 MW·cm^{-2}·sr^{-1} at an output power of 1.16 W.

OCIS codes: (070.6110) Spatial filtering; (140.2010) Diode laser arrays; (140.3298) Laser beam combining; (140.3410) Laser resonators; (140.5960) Semiconductor lasers.

References and links

1. I. P. G. Photonics, http://www.ipgphotonics.com.
2. N. Lichtenstein, B. E. Schmidt, A. Fily, S. Weiss, S. Arlt, S. Pawlik, B. Sverdlov, J. Muller, and C. S. Harder, "DPSSL and FL pumps based on 980-nm telecom pump laser technology: changing the industry," Proc. SPIE **5336**, 77–83 (2004).
3. J. P. Donnelly, R. K. Huang, J. N. Walpole, L. J. Missaggia, C. T. Harris, J. Plant, R. J. Bailey, D. E. Mull, W. D. Goodhue, and G. W. Turner, "AlGaAs-InGaAs slab-coupled optical waveguide lasers," IEEE J. Quantum Electron. **39**(2), 289–298 (2003).
4. P. Friedmann, J. Schleife, M. Herbstritt, J. Gilly, and M. T. Kelemen, "High efficiency laser sources usable for single mode fiber coupling and frequency doubling," Proc. SPIE **8277**, 82771M, 82771M-10 (2012).
5. H. Taniguchi, H. Ishii, R. Minato, Y. Ohki, T. Namegaya, and A. Kasukawa, "25-W 915-nm lasers with window structure fabricated by impurity-free vacancy disordering (IFVD)," IEEE J. Sel. Top. Quantum Electron. **13**(5), 1176–1179 (2007).
6. P. A. Crump, M. Grimshaw, J. Wang, W. Dong, S. Zhang, S. Das, J. Farmer, M. DeVito, L. S. Meng, and J. K. Brasseur, "85% power conversion efficiency 975-nm broad area diode lasers at - 50°C, 76% at 10°C," in *Conference on Lasers and Electro-Optics/Quantum Electronics and Laser Science Conference and Photonic Applications Systems Technologies*, Technical Digest (CD) (Optical Society of America, 2006), paper JWB24.
7. R. Pandey, D. Merchen, D. Stapleton, S. Patterson, H. Kissel, W. Fassbender, and J. Biesenbach, "Advancements in high-power diode laser stacks for defense applications," Proc. SPIE **8381**, 83810G, 83810G-12 (2012).
8. P. Crump, S. Böldicke, C. M. Schultz, H. Ekhteraei, H. Wenzel, and G. Erbert, "Experimental and theoretical analysis of the dominant lateral waveguiding mechanism in 975 nm high power broad area diode lasers," Semicond. Sci. Technol. **27**(4), 045001 (2012).
9. R. R. Craig, L. W. Casperson, O. M. Stafsudd, J. J. J. Yang, G. A. Evans, and R. A. Davidheiser, "Etched-mirror unstable-resonator semiconductor lasers," Electron. Lett. **21**(2), 62–63 (1985).
10. V. Raab and R. Menzel, "External resonator design for high-power laser diodes that yields 400mW of TEM$_{00}$ power," Opt. Lett. **27**(3), 167–169 (2002).
11. A. Jechow, V. Raab, R. Menzel, M. Cenkier, S. Stry, and J. Sacher, "1 W tunable near diffraction limited light from a broad area laser diode in an external cavity with a line width of 1.7 MHz," Opt. Commun. **277**(1), 161–165 (2007).
12. M. Chi, B. Thestrup, and P. M. Petersen, "Self-injection locking of an extraordinarily wide broad-area diode laser with a 1000-microm-wide emitter," Opt. Lett. **30**(10), 1147–1149 (2005).
13. A. Heuer, A. Sagahti, A. Jechow, D. Skoczowsky, and R. Menzel, "Multi-wavelength, high spatial brightness operation of a phase-locked stripe-array diode laser," Laser Phys. **22**(1), 160–164 (2012).
14. S. Wolff, D. Messerschmidt, and H. Fouckhardt, "Fourier-optical selection of higher order transverse modes in broad area lasers," Opt. Express **5**(3), 32–37 (1999).
15. J. R. Leger, "Lateral mode control of an AlGaAs laser array in a Talbot cavity," Appl. Phys. Lett. **55**(4), 334–336 (1989).
16. B. Liu, Y. Liu, and Y. Braiman, "Coherent beam combining of high power broad-area laser diode array with a closed-V-shape external Talbot cavity," Opt. Express **18**(7), 7361–7368 (2010).

17. T. Y. Fan, "Laser beam combining for high-power, high-radiance sources," IEEE J. Sel. Top. Quantum Electron. **11**(3), 567–577 (2005).
18. D. Vijayakumar, O. B. Jensen, and B. Thestrup, "980 nm high brightness external cavity broad area diode laser bar," Opt. Express **17**(7), 5684–5690 (2009).
19. M. Fukuda, M. Okayasu, J. Temmyo, and J. Nakano, "Degradation behavior of 0.98-μm strained quantum well InGaAs/AlGaAs lasers under high-power operation," IEEE J. Quantum Electron. **30**(2), 471–476 (1994).
20. V. Daneu, A. Sanchez, T. Y. Fan, H. K. Choi, G. W. Turner, and C. C. Cook, "Spectral beam combining of a broad-stripe diode laser array in an external cavity," Opt. Lett. **25**(6), 405–407 (2000).
21. A. I. Bawamia, B. Eppich, K. Paschke, H. Wenzel, F. Schnieder, G. Erbert, and G. Tränkle, "Experimental determination of the thermal lens parameters in a broad area semiconductor laser amplifier," Appl. Phys. B **97**(1), 95–101 (2009).
22. A. E. Siegman, "How to (maybe) measure laser beam quality," in *DPSS (Diode Pumped Solid State) Lasers: Applications and Issues*, Vol. 17 of OSA Trends in Optics and Photonics (Optical Society of America, 1998), paper MQ1.

1. Introduction

High power laser sources with good spatial beam quality are desirable for many applications including printing and marking, pumping of solid state lasers, imaging and tracking, and for use in nonlinear optical processes including optical parametric amplification and difference frequency generation. Fiber lasers are a top contender for high power applications requiring excellent beam quality, with commercially available fiber lasers producing kilowatt single-mode output powers and wall-plug efficiencies of ~30% [1]. However, fiber lasers require optically pumping with high power semiconductor diode lasers, fundamentally limiting the efficiency and power. Diode lasers themselves are a particularly attractive source platform as they offer a cheap, simple, compact, and efficient means to generate laser output across a broad spectrum, spanning the visible to the mid-infrared, directly from electrical current. While single-mode laser diodes are commercially available, continuous wave output powers remain limited to a few watts [2,3] due to high irradiances resulting from the small transverse dimensions required for single spatial mode operation. Tapered amplifiers can be used in conjunction with single mode laser diodes to increase continuous-wave powers up to several watts [4]. On the other hand, broad-area laser (BAL) diodes can produce continuous-wave powers in excess of 10 W [5], and have found utility in applications including cutting and welding and as high-power pump sources for fiber and solid state laser systems. Electrical-to-optical efficiencies exceeding 76% have been demonstrated at 980 nm [6]. Furthermore, multiple BALs can easily be fabricated on a single chip to create arrays, bars, and stacks that can produce kilowatt-level output powers [7]. However, BALs have inherently large lateral dimensions (100s of microns) and support multiple transverse modes [8]. Multimode emission reduces beam quality and precludes use in applications requiring conventional mode-locking or diffraction-limited spatial resolution.

External cavities provide a means to spatially and spectrally control feedback to diode lasers beyond the intrinsic feedback produced from monolithic structures. Improvements in the beam quality of BALs have been demonstrated using external cavities which employ unstable resonator structures [9], off-axis optical feedback [10–12], intracavity spatial filtering [13,14], and phase locking via the Talbot effect [15,16]. Using these external cavity techniques, the output from individual emitters within a BAL array can be spatially combined to produce a single output beam with increased total spatial radiance or brightness (power per square area per solid angle) [17]. Brightnesses as high as 79 MW·cm^{-2}·sr^{-1} [18] have now been demonstrated at 980 nm from a BAL array in an external cavity. While demonstrated external cavity techniques can improve BAL beam quality, the cavities are relatively complex and have limited usable current ranges or limited potential for beam combing. Talbot cavities can only be implemented through coherent beam combining as they produce phase-locking of adjacent emitters. Off-axis cavities show reduced electrical-to-optical efficiencies due to mismatch of the double-lobed output mode with the truncated output mode used for feedback and the gain profile [10]. Unstable resonators typically require additional nontrivial etching of diode facets [9].

In this paper, a new technique to improve the beam quality from BALs is demonstrated. The diffraction-limited fast-axis mode of the BAL is imaged onto the slow-axis facet, resulting in a twofold reduction of the slow-axis (combined) M^2 value and a corresponding twofold increase in brightness compared with a standard Littman-Metcalf wavelength beam combined cavity. The method is versatile and broadly applicable to BAL single emitters and arrays employing either coherent or wavelength beam combining.

2. Laser concept

The maximum output power from a single BAL is ultimately limited by either thermal roll-over or catastrophic optical damage. Thermal roll-over results from heating of the diode junction causing increased leakage current. Catastrophic optical damage is caused by nonradiative surface recombination at the diode facet [19]. To avoid these limitations and reach higher optical powers, multiple BALs can be placed side-by-side in a tiling arrangement. While tiling increases the total output power by a factor equal to the number of emitters, the spatial radiance or brightness remains equal to that of a single BAL [17]. The brightness can be increased if each laser's output is spatially overlapped. Beam combining schemes accomplish this by controlling the phase or frequency of the emitters. The result is scaling of the output power and brightness in proportion to the number of emitters [17]. In coherent beam combing, multiple lasers are forced to operate at the same wavelength, and the relative phase of the output emitted by each laser is locked. Wavelength beam combining (WBC) is analogous to wavelength-division-multiplexing in fiber and relies on locking each laser to a different wavelength and spatially combining the outputs into a single beam. Typically, the beams from individual elements are spatially overlapped using a lens and a diffraction grating. The resulting beam has increased spatial radiance at the expense of reduced spectral radiance (power per square area per solid angle per wavelength). To increase the brightness of a WBC source, one can either increase the number of individual laser sources being combined or improve the beam quality produced from each emitter. Using mode imaging in a WBC cavity the beam quality produced from each emitter within a BAL array has been improved, allowing a maximum brightness of more than 45 MW·cm^{-2}·sr^{-1} to be achieved at an output power of > 1 W. Performance was compared to a standard WBC cavity with and without an intracavity slow-axis spatial mode filter. The maximum brightness of the mode-imaging WBC cavity is found to represent nearly a twofold increase in brightness over a similar standard WBC cavity without any mode filtering.

All three WBC cavity configurations use an anti-reflection-coated BAL array containing nineteen 100-μm wide emitters with a center-to-center separation of 500 μm (Jenoptik). The basis of all three cavity configurations is illustrated in Fig. 1(a). First, the fast and slow axes of the array are collimated. In the slow axis, the collimated beam from each emitter is then imaged onto an 1800 lines/mm holographic diffraction grating using a 100-mm focal length transform lens placed one focal length away from both the array and the diffraction grating. Together, the element-to-element spacing of the array, the focal length of the transform lens, and the groove density and diffraction angle of the grating determine the spectral content of the combined output [20]. The first-order diffracted light then passes through a 500-mm focal length secondary fast-axis collimating lens which minimizes the beam divergence in the fast axis. Next, a 1.5:1 slow-axis telescope is used to shrink the slow-axis waist of the beam to more closely match the waist in the fast axis, reducing beam astigmatism. Efficient operation of the mode-imaging cavity requires the described astigmatism correction. An adjustable slit is placed at the focus of the slow-axis telescope. This slit can be left open or closed to a width of 130 μm ± 25 μm and used as an intracavity slow-axis mode filter. Following the slow-axis telescope is an uncoated 3° BK7 wedge used to pick off portions of the combined beam for beam quality and spectral measurements. In the case of the mode-imaging cavity, the dashed box in Fig. 1(a) contains the loop mirror shown in Fig. 1(b). In this configuration, the intracavity slit is left open, and the output power is measured using the zeroth-order diffracted light off of the grating from the returning, spatially-combined beam. In the case of the standard cavities, the dashed box contains only a 30% reflective flat output coupler and a
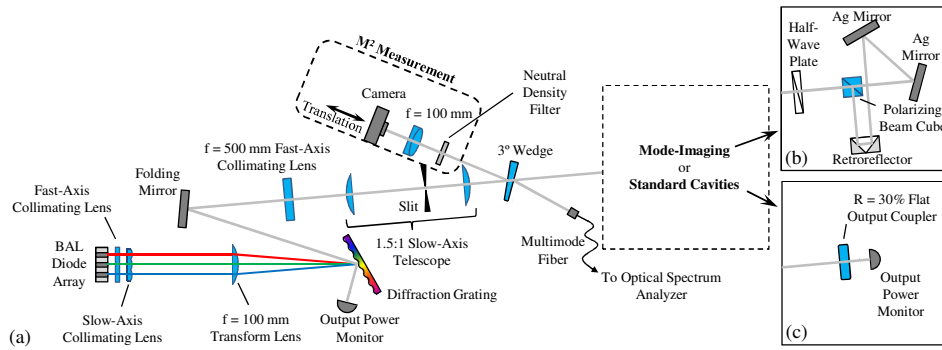
Fig. 1. Standard and mode-imaging wavelength beam combined (WBC) cavities. (a) Basis of both the standard and mode-imaging cavities. The 500-mm focal length secondary fast-axis collimating lens minimizes the fast-axis beam divergence while the 1.5:1 slow-axis telescope reduces the beam waist in the slow axis to approximately 90% of the collimated fast-axis beam waist. (b) Loop mirror used to switch fast- and slow-axis modes. The retroreflector is used as a right-angle prism with the reflection axis rotated 45° relative to the fast and slow axis of the incident beam. (c) Flat output coupler followed by thermal head used to measure output power for the standard WBC cavities.

thermal head used to measure the total output power of the combined beam, as shown in Fig. 1(c). Both the mode-imaging cavity and the standard cavities are relatively long, with effective lengths of 1.7 m and 1.3 m, respectively.

The loop mirror is used to swap the fast- and slow-axis modes emitted from the array and is comprised of a half-wave plate, polarizing beam cube, hollow metal retroreflector, and two silver steering mirrors. The retroreflector is used as a right-angle prism with light reflected by only two sides. The 90° intersection of the two sides represents the reflection axis for the incident beam. The reflection axis is oriented perpendicular to the propagation direction of the incident beam and rotated 45° relative to the fast and slow axis of the BAL emitters. Figure 2 illustrates the mechanism for swapping the fast- and slow-axis spatial modes with the retroreflector. For simplicity, the beam is depicted as astigmatic and centered on the retroreflector's reflection axis. In the actual implementation of the loop mirror, the beam is well off-axis, on the retroreflector. The two silver steering mirrors are then used to overlap this shifted beam with the incident beam on the polarizing beam cube. The result of the loop mirror is that the near single-mode fast-axis beam is rotated 90° and imaged back upon the much larger slow-axis facet, and vice versa. This results in increased feedback to the fundamental mode supported in the slow axis of the broad area emitters and suppression of the higher order modes which have less spatial overlap with the ~1 μm wide fast-axis mode.

For maximum feedback to the laser diodes, the half-wave plate is set to rotate the transverse electric (TE) polarization (parallel to the slow axis) amplified by the laser diodes by 45° as shown in Fig. 2(a). The polarization at the retroreflector is now parallel to the 90° intersection of the two sides of the retroreflector. Now the polarization is invariant when the fast- and slow-axis spatial modes are swapped during retroreflection as indicated in Fig. 2(b). The polarization of the retroreflected beam remains identical to that of the incident beam as it is rotated back to purely TE by the half-wave plate, as shown in Fig. 2(c), allowing all of the retroreflected light to be amplified by the BAL emitters. While the holographic grating used has a diffraction efficiency of ~90% for the TE polarized light emitted by the laser diodes, the diffraction efficiency for the transverse magnetic (TM) polarized light is only ~10%. Therefore, the TM component of the retroreflected light is outcoupled directly from the zeroth-order retroreflected beam off of the grating with ~90% efficiency. By rotating the half-wave plate, the grating can be used as a variable reflectivity output coupler. Since only the TE polarization component of the retroreflected beam is amplified, controlling the amount of retroreflected light that is TE polarized controls the feedback. Some TM light that cannot be amplified is always incident on the array elements. While this was not a problem for the ~1 W
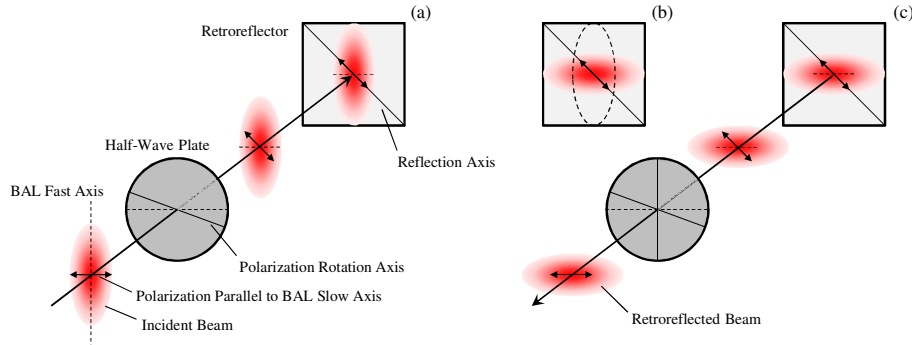
Fig. 2. Diagram illustrating mode swapping with retroreflector. (a) For maximum feedback the half-wave plate rotates the TE polarization of the incident beam to be parallel with the reflection axis of the retroreflector. (b) The beam reflects across the reflection axis of the retroreflector swapping the fast- and slow-axis spatial modes present in the incident beam. Since the polarization is parallel to the reflection axis, it remains unchanged after retroreflection. (c) The retroreflected beam passes back through the half-wave plate where the polarization is rotated back parallel to the TE polarization amplified by the laser diodes. The beam is depicted as astigmatic for clarity, but a stigmatic beam maximizes coupling of the retroreflected beam back into the fast- and slow-axis facets of the BAL emitters.

output powers measured here, at higher powers TM polarized light could cause excess heating in the BAL emitters and degrade the array's performance. This potential problem can be easily mitigated with an optimized grating or an additional polarizing beam splitter placed between the grating and the half-wave plate.

The retroreflector uses an off-axis reflection to provide feedback via the loop mirror. The off-axis implementation is used to prevent beam distortions in the retroreflected beam. When the incident beam is centered on the reflection axis, distortion is evident, as shown in Fig. 3(a). This can be compared with Fig. 3(b), showing an image of the beam reflected off-axis which looks nearly identical to the incident beam, shown in Fig. 3(c) for reference. For an on-axis reflection, interference between the two sides of the incident beam causes the distortion. The two sides of the retroreflector are not at exactly 90° (angular tolerance is specified as ± 2 arcseconds, equal to ± 0.01 mrad), and the two beams walk across each other after reflection.
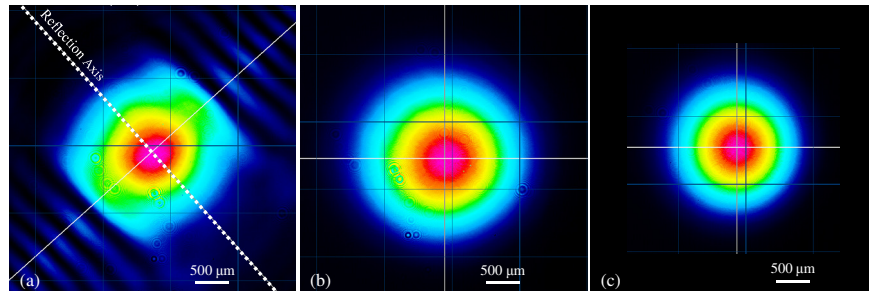

Fig. 3. Characterization of aberrations from the retroreflector. The highest and lowest intensities are shown magenta and black, respectively. Images were taken of a retroreflected HeNe beam with the incident beam centered (a) directly on the retroreflector's reflection axis and (b) far away from the reflection axis. (c) Image of the incident HeNe beam used to test the retroreflector. The beam distortion in (a) is due to interference between the two sides of the reflected beam. The two sides walk across each other due to the imperfect 90° angle between the two reflecting surfaces.

3. Results and discussion

Optical spectra, power, and beam quality were measured for all three WBC cavity configurations. Together, these measured quantities are used to compare the brightness

achieved for each configuration. In the mode-imaging cavity, the distance between the lenses used in the 1.5:1 slow-axis telescope is re-optimized for output powers greater than 1 W (currents > 8 A). Increasing the separation between the telescope lenses with larger drive currents optimized the output power and beam quality. The optimal separation increased monotonically over the range of currents investigated, reaching a maximum of 8 mm at 11 A and 1.62 W output power. The behavior suggests the formation of a thermal lens within the BAL emitters [21] and increased overlap of higher order modes with the gain profile within the emitters relative to overlap of the fundamental mode.

An output spectrum from the mode-imaging WBC cavity is shown in Fig. 4(a). The spectrum shows multiple individual emission peaks within a bandwidth of about 25 nm. Each emission peak is produced from one emitter in the array. The center wavelength of each peak is determined by the array pitch and cavity optics, and depends on the incident and diffraction angle of the beam from each emitter relative to the grating [20]. The output spectra for all three laser configurations are nearly identical.

The L-I characteristics for all three laser cavity configurations are shown in Fig. 4(b). The threshold current and slope efficiency are 4.1 A and 0.42 W/A, respectively, for the standard Littman-Metcalf WBC cavity without any mode filtering. The threshold currents for both the standard cavity with intracavity mode filtering and the mode-imaging cavity are similar, and the slope efficiencies are nearly identical at 0.26 W/A and 0.24 W/A, respectively. The standard cavity with the intracavity mode filter did not generate output powers beyond 1.02 W even for currents above 8.5 A. This corresponds to the same current where optimization of the slow-axis telescope becomes necessary in the mode-imaging cavity. Thermal lens formation within the BAL emitters may cause reduced transmission through the intracavity slit. Additionally, the anti-reflection coating on the BAL array is imperfect, and drive currents of ~10 A correspond to chip-mode lasing without an external cavity. At 8.5 A, the gain in the fundamental external cavity mode may become equal to the gain of the higher-order chip modes. Further increasing the current would increase the relative gain for the chip modes and thus cause a reduction in the observed power in the fundamental mode circulating within the external cavity.

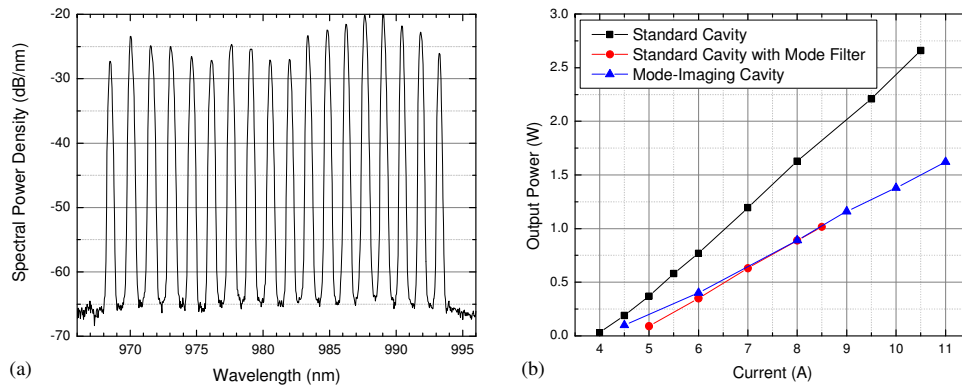(a)   (b)

Fig. 4. (a) Spectrum from the mode-imaging cavity taken at a drive current of 9 A producing 1.16 W of output power. The spectrum is typical of all the wavelength beam combined (WBC) laser cavities investigated. Each emission peak corresponds to one emitter in the array with center wavelengths determined by the particular incident and first-order diffraction angle from the grating. The centroid of the spectrum is at 983 nm. (b) L-I curves for the standard WBC cavity without (black squares) and with (red circles) a 130-μm wide intracavity slit used for mode filtering and for the mode-imaging cavity (blue upward pointing triangles).

The beam quality is determined by focusing the beam reflected from the uncoated 3° wedge with a 100-mm focal length achromatic doublet lens and measuring the fast- and slow-axis beam waists with a CMOS camera at several positions. The measured fast- and slow-axis beam caustics were fit using the standard hyperbolic equation [22] with the minimum waist, the axial position corresponding to the minimum waist, and the M^2 factor as free parameters.

The fast-axis M^2 values range from 1.2 to 1.4 for all cavity configurations, and the measured slow-axis beam quality as a function of output power for all three cavity configurations is shown in Fig. 5(a). The slow-axis M^2 increases with output power for all cavity configurations. Both the standard WBC cavity with mode filter (red circles) and the mode-imaging cavity (blue triangles) show dramatic improvement in beam quality over the standard cavity with no mode filtering. While both cavity configurations show similar trends for the measured slow-axis M^2 values, the standard cavity with slow-axis mode filtering could not generate output powers beyond ~1 W. However, the mode-imaging cavity data shows that the M^2 values remain low until an output power of 1.16 W is reached, after which the beam quality quickly degrades. The drive current corresponding to these transitions coincides closely with the threshold current for lasing observed for the BAL array without any external cavity feedback. Improving the anti-reflection coating on the front facet of the diodes or angle cleaving the laser facets should permit higher powers to be reached before observing substantial degradation in the beam quality.

The radiance or brightness, B, of the WBC lasers is given by [17],

$$ B = \frac{P}{\lambda^2 M_x^{\,2} M_y^{\,2}}, \qquad (1) $$

where P is the output power, λ is the center wavelength, and M_x^2 and M_y^2 are the slow- and fast-axis M^2 values. Brightness computed using Eq. (1) as a function of total output power for all three cavity configurations is shown in Fig. 5(b). Again, the standard cavity with mode filtering and the mode-imaging cavity are seen to have similar brightness for output powers up to ~1 W, reaching peak values in excess of 45 MW·cm^{-2}·sr^{-1}, approximately a factor of two more than that of the standard cavity without mode filtering at the same output power. The brightness for the mode-imaging cavity is seen to degrade at output powers beyond 1.16 W as a direct consequence of the rapid increase in the slow-axis M^2 values.
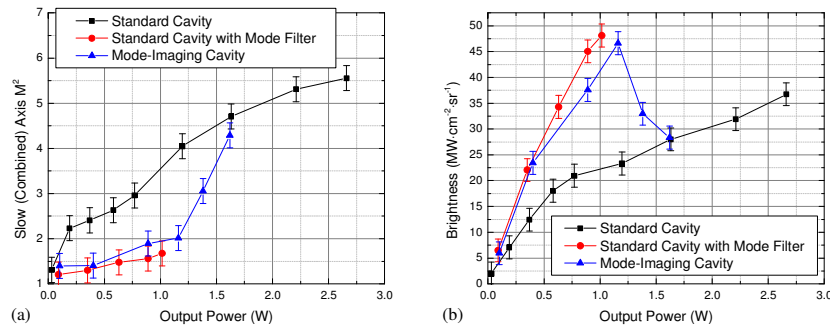

Fig. 5. (a) Average slow-axis beam quality as a function of output power for the standard wavelength beam combined (WBC) cavity without (black squares) and with (red circles) intracavity mode filtering and for the mode-imaging cavity (blue upward pointing triangles). Slow-axis M^2 values for both the standard cavity employing mode filtering and the mode-imaging cavities are improved over the standard cavity without mode filtering, and follow very similar trends with the notable exception that the standard cavity with mode filtering could not generate output powers beyond ~1 W. (b) Average brightness as a function of output power for all three cavity configurations. The standard WBC cavity employing mode filtering (red circles) and the mode-imaging cavity (blue upward pointing triangles) show maximum brightnesses of greater than 45 MW·cm^{-2}·sr^{-1}. Error bars indicate ± one standard deviation from multiple measurements as determined from the cavity configuration with the highest measured standard deviation.

4. Conclusion

A novel technique to dramatically improve beam quality produced from BALs in which the emitted fast-axis mode is reimaged back onto the slow-axis dimension of the laser facet has

been demonstrated. Together, the fast-axis lens and BAL facets function as optical Fourier filters, suppressing lasing of higher-order transverse modes within the external cavity. The technique is simple and broadly applicable to BAL single emitters and arrays employing external cavity feedback, including both coherent and wavelength beam combined systems. Slow-axis M^2 values of ≤ 2 at output powers up to 1.16 W have been achieved from a BAL array in a WBC cavity employing this mode-imaging technique, producing a maximum brightness of 47 $MW \cdot cm^{-2} \cdot sr^{-1}$ at a center wavelength of 983 nm. The beam quality improvement from the mode-imaging cavity configuration closely parallels that observed from a standard WBC cavity employing a slow-axis telescope and slit as an optical Fourier filter due to filtering characteristics of the mode-imaging cavity. To the authors' knowledge, this work represents the first application of intracavity Fourier filtering to an array of single-stripe BAL emitters, with demonstrated output powers and brightnesses in excess of those reported for the near single mode emitters within the multi-stripe array used in [13].

Both intracavity Fourier filtering and the newly demonstrated mode-imaging technique have been demonstrated to improve the beam quality from a BAL array within a WBC setup. The mode-imaging technique achieved ~20% higher output power compared with the mode filter cavity before significant beam quality degradation was observed. Simplifying the mode-imaging cavity setup by employing fewer optical components may further increase the maximum output power and brightness. For example, utilizing matched fast- and slow-axis collimating lenses which produce astigmatic beams directly from the emitters would allow the secondary fast-axis collimating lens and the two slow-axis telescope lenses to be removed from the current setup. Fewer optics and better fast- and slow-axis mode matching would reduce intracavity losses, provide simpler and more robust cavity alignment, and allow much shorter cavity lengths to be realized. At high powers, competition from chip-mode lasing is expected to spoil the beam quality. Increasing the lasing threshold of the BAL array through better anti-reflection coatings or utilizing emitters with angled facets should increase the usable output power and maximum brightness.

Acknowledgments